ACS APPLIED MATERIALS & INTERFACES

Critical Role of Perovskite Film Stoichiometry in Determining Solar Cell Operational Stability: a Study on the Effects of Volatile A-Cation Additives

Wenya Song,$^{\bigcirc}$ Xin Zhang,$^{\bigcirc}$ Stijn Lammar,$^{\bigcirc}$ Weiming Qiu,* Yinghuan Kuang,* Bart Ruttens, Jan D'Haen, Inge Vaesen, Thierry Conard, Yaser Abdulraheem, Tom Aernouts, Yiqiang Zhan, and Jef Poortmans*

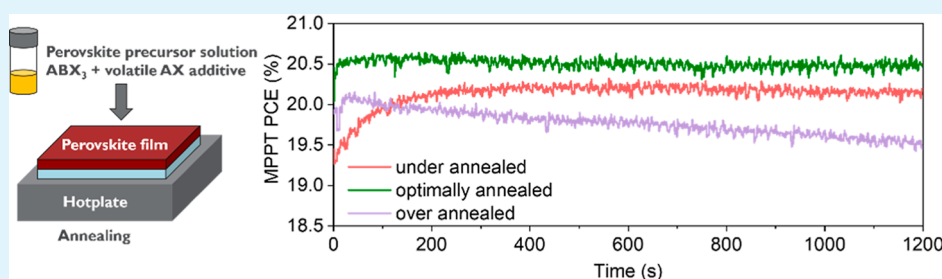Read Online

ACCESS | 📊 Metrics & More | 📰 Article Recommendations | 🆂�🅸 Supporting Information

ABSTRACT: Volatile A-cation halide (AX) additives such as formamidinium chloride and methylammonium chloride have been widely employed for high-efficiency perovskite solar cells (PSCs). However, it remains unstudied how they influence the perovskite film stoichiometry and the solar cell performance and operational stability. Hereby, our work shows that over annealing of formamidinium chloride-containing perovskite films leads to a Pb-rich surface, resulting in a high initial efficiency, which however decays during maximum power point tracking (MPPT). On the contrary, perovskite films obtained by a shorter annealing time at the same temperature provide good stability during MPPT but a lower initial efficiency. Thus, we deduce that an optimal annealing is vital for both high efficiency and operational stability, which is then confirmed in the case where methylammonium chloride additive is used. With optimized perovskite annealing conditions, we demonstrate efficient and stable p−i−n PSCs that show a best power conversion efficiency of 20.7% and remain 90% of the initial performance after a 200 h MPPT at 60 °C under simulated 1 sun illumination with high UV content. Our work presents a comprehensive understanding on how volatile AX impacts perovskite film stoichiometry and its correlation to the device performance and operational stability, providing a new guideline for fabricating high-efficiency and operationally stable PSCs.

KEYWORDS: perovskite solar cells, operational stability, additive, stoichiometry, maximum power point tracking

1. INTRODUCTION

Organometal halide perovskite solar cells (PSCs) have achieved more than 25% efficiency[1−4] and their operational stability has also seen significant progress.[5−8] However, the root causes of device degradation under operation are still not fully understood which is critical for further improvement of device operational stability. Previous studies have shown that the composition of perovskite films plays a crucial role in determining device stability.[6,9] On the one hand, it is generally believed that methylammonium-free perovskites, for example, formamidinium cesium cation-based perovskites, are more stable than the ones containing methylammonium cation (MA$^+$), due to the volatile nature of MA compound that changes the perovskite film stoichiometry.[10,11] On the other hand, volatile additives such as formamidinium chloride (FACl)[12−14] and methylammonium chloride (MACl)[15−19]

have been widely used to achieve high-efficiency PSCs because they could optimize the perovskite crystal formation dynamics.[17,20] This brings the scientific question currently scarcely studied, that is, how such volatile additives influence the perovskite film stoichiometry and how this correlates to the device performance and operational stability.

We first carried out our investigation on the gas-quenched perovskite films with a nominal composition of $Cs_{0.1}FA_{0.9}PbI_{2.865}Br_{0.135}$ which were prepared with volatile
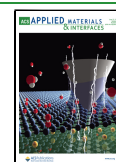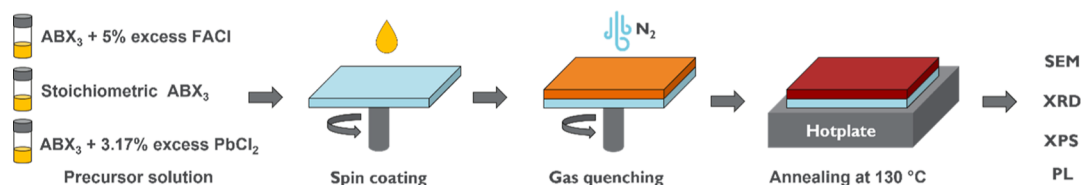
Figure 1. Schematic representation of the processing procedures of perovskite films and the characterizations performed on the films.

FACl as the additive. By changing the thermal annealing time during film processing, the stoichiometry of the perovskite film can be well controlled. This enables us to link the film stoichiometry to the device operational stability. Our results show that an optimal annealing condition is crucial to achieve both high efficiency and long-term stability. The over annealing of perovskite film with volatile A-cation additives results in an A-cation deficiency or in other words a Pb-rich surface, which leads to a high initial power conversion efficiency (PCE). However, these kinds of high-PCE solar cells degrade fast under the solar cell operational maximum power point tracking (MPPT) condition. On the contrary, perovskite films obtained from less annealing time at the same temperature provide good stability under MPPT but at a lower initial efficiency. The same trend is then further confirmed in the case where MACl is used as the additive. With careful control on the thermal annealing condition, we demonstrate efficient and stable PSCs that show a best PCE of 20.7% and remain 90% of the initial performance after MPPT tracking for 200 h at 60 °C under 1 sun illumination with high UV content. Our work presents a comprehensive understanding on the role of volatile additives on the perovskite film stoichiometry and its correlation to the device performance and operational stability, providing a new guideline for the fabrication of high-efficiency and operationally stable PSCs.

2. RESULTS AND DISCUSSION

2.1. Stoichiometry Control of Perovskite Films. In this study, we employed the dual-cation perovskite films with a nominal ABX_3 composition of $Cs_{0.1}FA_{0.9}PbI_{2.865}Br_{0.135}$ on glass/ITO/poly[bis(4-phenyl) (2,4,6-trimethylphenyl) amine] (PTAA) substrates, fabricated from a gas-quenching method as shown in Figure 1. The perovskite films with volatile FACl additive were prepared from the precursor solution with 5 mol % excess FACl compared to the stoichiometric ABX_3 composition (denoted as ABX_3 + 5% excess FACl). To investigate the influence of thermal annealing condition on perovskite stoichiometry, we annealed the as-prepared films made from the same solution at 130 °C for 1 min, 5 min, 10 min, 20 min, 30 min, and 40 min in a N_2-filled glovebox, respectively. Furthermore, two reference films were prepared, respectively, from stoichiometric precursor solution without any additive (denoted as ABX_3) and with 3.17 mol % extra $PbCl_2$ (denoted as ABX_3 + 3.17% excess $PbCl_2$). The reference films were both annealed at 130 °C for 10 min. This way, we covered precursor solution formulas from ABX_3 + excess AX to stoichiometric ABX_3 and further to ABX_3 + excess BX_2. The materials, solution preparation methods, and film processing details can be found in Table 1 and Sections 4.1.2 and 4.1.3., respectively. Scanning electron microscopy (SEM), X-ray diffraction (XRD), X-ray photoelectron spectroscopy (XPS), and photoluminescence (PL) measurements were carried out to examine morphology, crystallinity, and stoichiometry of the films.

Table 1. Materials and Their Supplying Companies Used in This Work

materials	company
indium tin oxide (ITO)-coated glass substrates	Colorado Concept Coatings LLC
lead iodide (PbI_2)	Tokyo Chemical Industry (TCI)
lead chloride ($PbCl_2$)	Sigma-Aldrich
formamidinium iodide (FAI)	Greatcell Solar Materials
formamidinium bromide (FABr)	Greatcell Solar Materials
cesium iodide (CsI)	Tokyo Chemical Industry (TCI)
methylammonium chloride (MACl)	Shanghai MaterWin
fullerene C_{60}	Nano-C
bathocuproine (BCP)	Luminescence Technology Corp. (Lumtec)
poly[bis(4-phenyl)(2,4,6-trimethylphenyl) amine] (PTAA)	Flexink
lithium fluoride (LiF)	Sigma-Aldrich
magnesium difluoride (MgF_2)	Angstrom Engineering
copper (Cu)	Angstrom Engineering
anhydrous N,N-dimethylformamide anhydrous, 99.8% (DMF)	Sigma-Aldrich
anhydrous 1-methyl-2-pyrrolidone (NMP)	Sigma-Aldrich
anhydrous isopropanol (IPA)	Sigma-Aldrich
anhydrous toluene	Sigma-Aldrich

Figure 2 shows the secondary electron SEM images of the eight films mentioned above. Plate-like phases are present on stoichiometric and 3.17% excess $PbCl_2$ films (Figure 2g,h). Positions of these plate-like phases correspond to bright phases in Inlens SEM images (Figures S1, S2g,h). According to previous studies, such bright phases often represent PbI_2.[21−24] On the contrary, the plate-like phases are absent in all the films prepared with 5% excess FACl solution and annealed for 1−40 min (Figure 2a−f). However, it is noticeable that as the annealing time increases, the surface morphology of 5% excess FACl films changes. The 5% excess FACl 30 min film started to show fringes on perovskite grains (Figure 2e). Flat grain surfaces appeared on the 5% excess FACl 40 min film (Figure 2f).

Figure 3a shows the XRD patterns of these eight films. All the films show main diffraction peaks at 14.0°, 28.3°, and 31.7°, indicating the (001), (002), and (012) planes of cubic-phase perovskites.[25−28] The lattice constants of all these perovskite films are 6.32 Å, indicating that the added Cl after film annealing has little impact on perovskite crystal structure. The stoichiometric 10 min film and the 3.17% excess $PbCl_2$ film both show diffraction peaks at 12.7°, which is classified as the (001) peak in cubic-phase PbI_2.[29−31] The PbI_2 peak intensity in the stoichiometric 10 min film is less than that of the 3.17% excess $PbCl_2$ 10 min film, just as the flake amount in the stoichiometric 10 min film is less than that in the 3.17% excess $PbCl_2$ film. In the meantime, the $PbBr_2$ and $PbCl_2$ characteristic XRD peaks are not observed.[29] Thus, we can
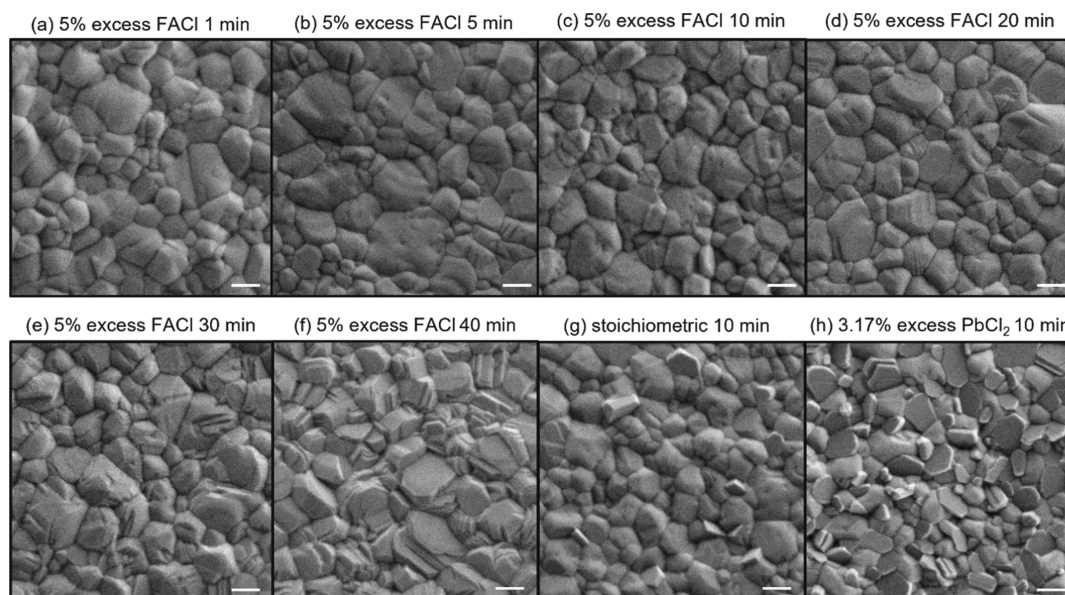
Figure 2. (a−h) Secondary electron mode SEM images of the corresponding perovskite films. The length of the scale bars indicates 200 nm.
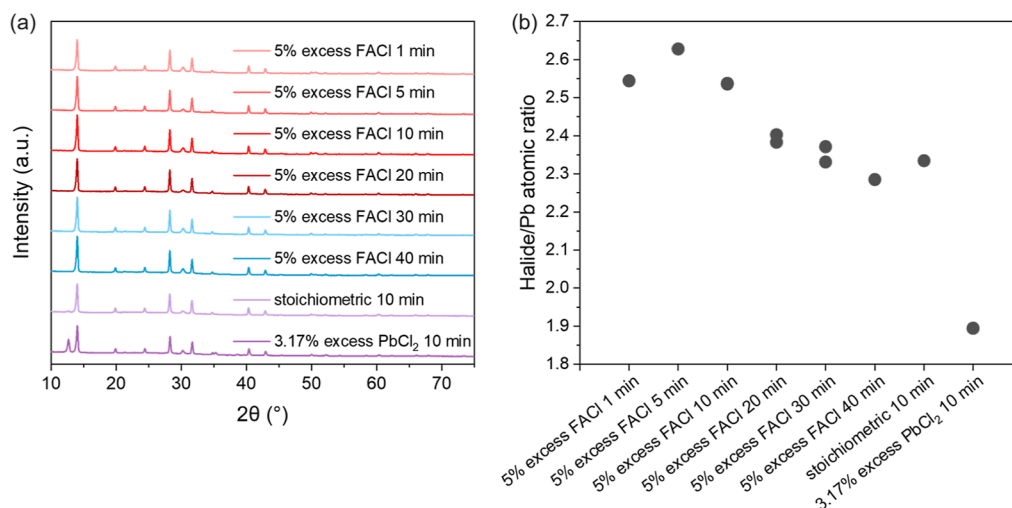

Figure 3. (a) XRD patterns and (b) halide/Pb atomic ratios from XPS measurements of the eight types of perovskite films. Two films from 5% excess FACl 10 min, 20 min, and 30 min conditions were measured, respectively. These data points illustrate reproducibility in XPS measurements. To note, the two data points for 5% excess FACl 10 min films completely overlap.

safely deduce that the plate-like phases as shown in Figure 2g,h are PbI_2.

Figure 3b shows the halide/Pb atomic ratio calculated from XPS measurements. The total halide amount sums the amount of iodide, bromide, and chloride. The Pb amount sums the amount of both Pb^{2+} and metallic Pb. The $4f_{7/2}$ Pb signals from XPS measurements of each perovskite films are shown in Figure S3, where the peaks at 138.4 eV originate from Pb^{2+}, and the peaks at 136.6 eV are associated with metallic Pb.[32] According to precedent studies,[11,33,34] the metallic Pb is detected due to the photolysis of PbX_2 into Pb and X_2 under X-ray. To note, under X-ray irradiation, ABX_3 perovskite also decomposes into PbX_2, which can further decompose to Pb.[33] Thus, it is reasonable that the halide/Pb ratio of the perovskite surface is lower than 3. As we can see from Figure 3b, the 3.17% excess $PbCl_2$ 10 min film shows the lowest halide/Pb ratio of 1.89 among all the films, suggesting this film has a large amount of PbX_2 at the surface. The stoichiometric 10 min film

shows a halide/Pb ratio of 2.33, implying that the surface of this film is a mixture of ABX_3 perovskite and PbX_2 and it has less PbX_2 compared to that in the 3.17% excess $PbCl_2$ 10 min film. These observations well align with those in SEM and XRD as shown in Figures 2g,h and 3a. We can observe a trend that as the annealing time of the 5% excess FACl films increases from 1 to 40 min, the halide/Pb ratio decreases from the highest point of 2.63 to the lowest point of 2.29. Despite the decreasing halide/Pb ratio, none of the 5% excess FACl films show PbI_2 signals in the XRD spectrum (Figure 3a), indicating that PbI_2 crystals are not formed. However, the SEM images in Figure 2a−f show that as the annealing time increases, the perovskite grain surface starts to show fringes and become flat. Thus, we can deduce that a Pb-rich perovskite crystal facet is likely formed as the annealing time of 5% excess FACl film increases, which leads to a low halide/Pb ratio at the surface.

Apart from deducing surface stoichiometry through a combination of SEM, XRD, and XPS, we also deduce the perovskite bulk stoichiometry from the band gap obtained from steady-state photoluminescence. Figure 4 shows the band
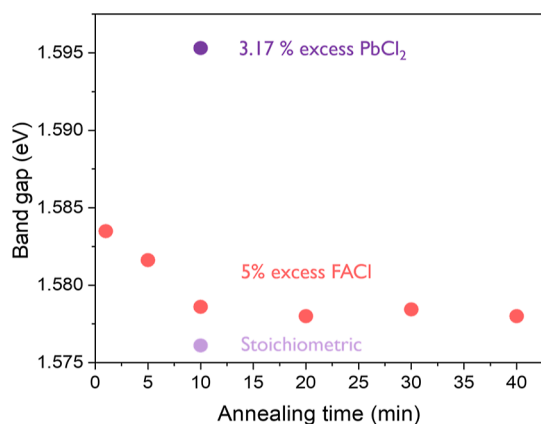

Figure 4. Band gap of the eight investigated perovskite films calculated from steady-state photoluminescence.

gap of stoichiometric 10 min and 3.17% excess PbCl$_2$ 10 min perovskite films are 1.576 eV and 1.595 eV, respectively. The band gap of 5% excess FACl films first decreases from 1.583 eV to 1.578 eV as the annealing time increases from 1 min to 10 min, then the band gap stabilizes around 1.578 eV as the annealing time increases from 10 min to 40 min. This trend suggests that in the beginning of annealing, most Cl is still incorporated in the perovskite crystals, leading to a high band gap.[35] As annealing time increases to 10 min, the amount of Cl in perovskites gradually reduces due to the evaporation of Cl-containing volatile species, leading to a decrease in the band gap. Once the Cl amount stabilizes in the perovskite film, the band gap of the film also stabilizes. We can deduce that once the annealing time exceeds 10 min the bulk stoichiometry likely remains unchanged.

Combining the SEM, XRD, XPS, and PL results, we can conclude that during the first 10 min of annealing at 130 °C, the bulk stoichiometry of the 5% excess FACl film changes. When the annealing time exceeds 10 min, the bulk stoichiometry of perovskite films stays unchanged, whereas the surface of perovskite becomes more Pb-rich. Hence, we can further conclude that it is possible to control the bulk and
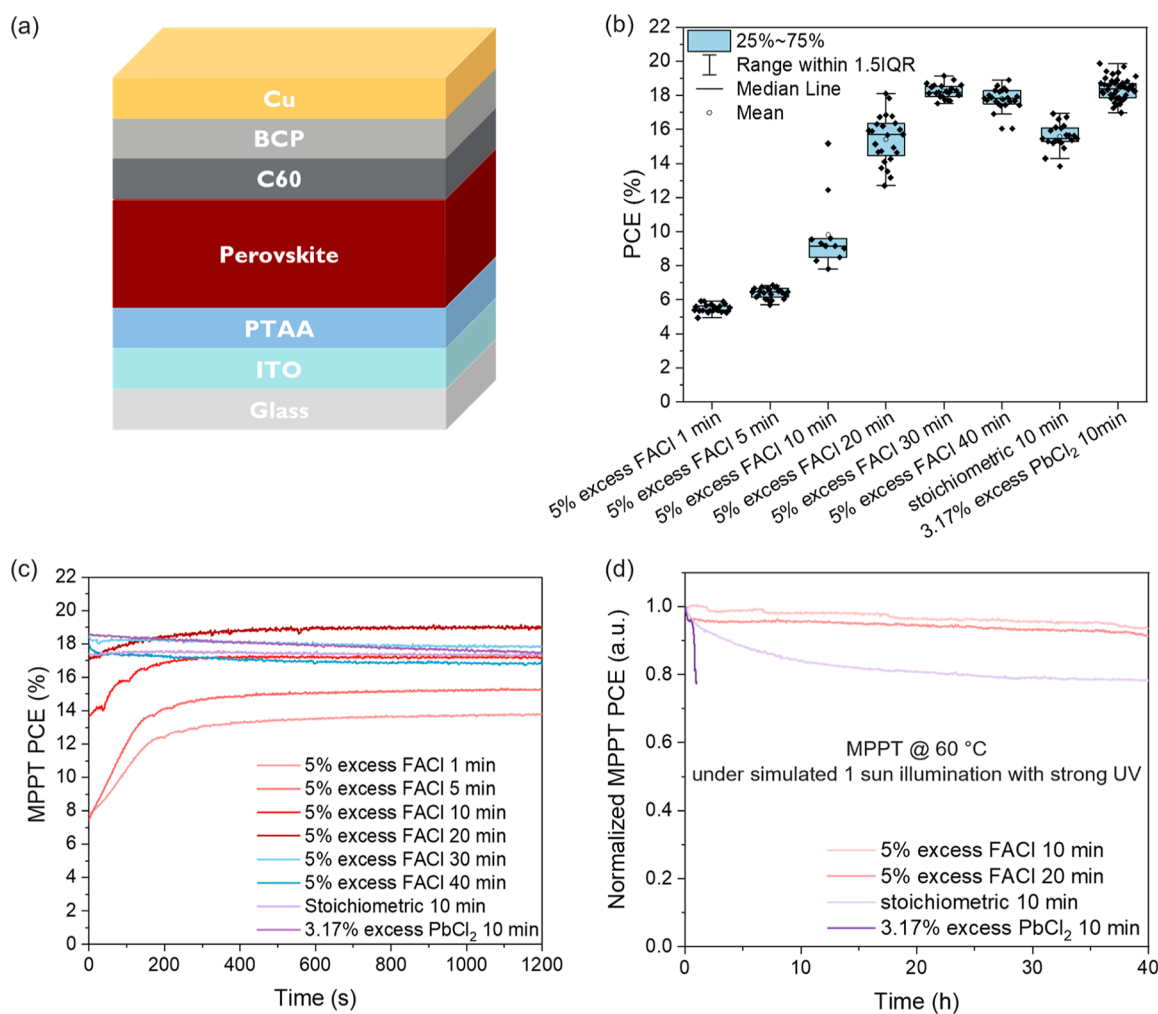

Figure 5. (a) Schematics of the PSC structure. (b) Initial PCE distribution of PSCs with corresponding perovskites films. (c) 20 min MPPT of PSCs under 1 sun xenon illumination lamp at 30 °C. (d) 40 h MPPT of the corresponding PSCs under simulated 1 sun illumination from a metal halide lamp, which contains strong UV content. The cell temperature reaches 60 °C.

Table 2. MPPT Conditions Used in This Work

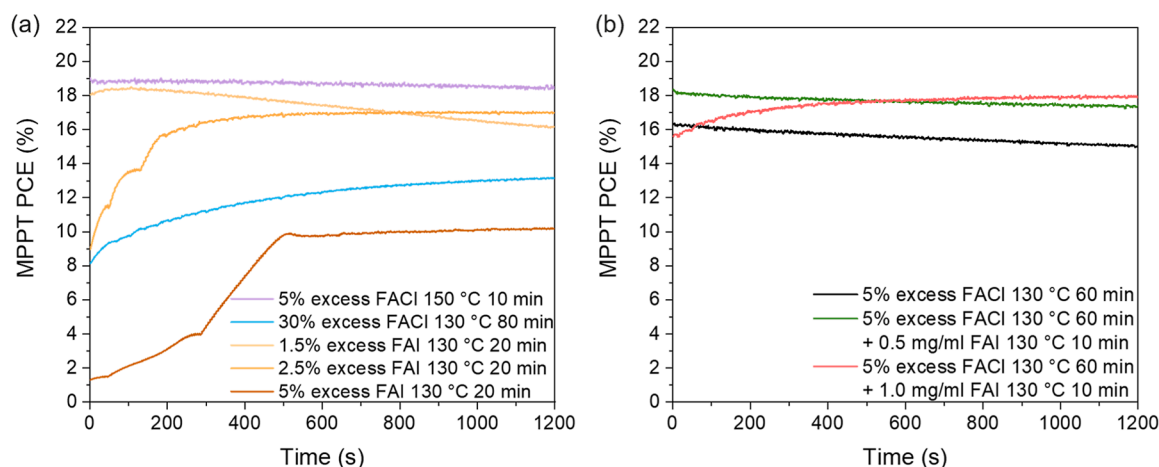|	ISOS test ID	light source	UV filter	intensity (Suns)	T (°C)	atmo-sphere	encap-sulation
20 min MPPT as shown in Figures 5c, 6, 7c	ISOS-L-1I	450 W xenon lamp (Abet Sun 3000) with AM1.5G illumination	no	1	30	N_2	no
long-term MPPT as shown in Figures 5d, 7f	ISOS-L-2I	1200 W metal halide lamp with simulated AM1.5G illumination	no	1	60	N_2	no

Figure 6. (a) 20 min MPPT of PSCs with corresponding processing conditions. (b) 20 min MPPT of PSCs with and without FAI surface treatment.

surface stoichiometry of perovskite films with volatile AX excess through simply controlling their annealing time.

2.2. Linking Perovskite Film Stoichiometry with Solar Cell Operational Stability. To unveil the relation between perovskite stoichiometry and solar cell operational stability, we fabricated solar cells with the structure of glass/ITO/PTAA/perovskite/C_{60}/BCP/Cu (Figure 5a), where perovskite layers are the eight types of films investigated in the previous section. The initial PCEs obtained from current density-voltage ($J-V$) scans in Figure 5b show that as the annealing time of 5% excess FACl perovskites increase from 1 to 40 min, the average initial PCE first increases from 5.5% (1 min) to 18.3% (30 min) and then drops to 17.8% (40 min). The average initial PCE of stoichiometric 10 min and 3.17% excess $PbCl_2$ 10 min perovskites are 15.6 and 18.4%, respectively. The rest parameters from $J-V$ scans are presented in Figure S4.

Interestingly, despite the higher initial PCE, the 3.17% excess $PbCl_2$ 10 min, stoichiometric 10 min, and 5% excess FACl 40 and 30 min PSCs all show declining PCE during the 20 min MPPT under 1 sun illumination from a xenon lamp (Figure 5c), owing to the decrease of voltage at maximum power point (V_{mpp}) as can be seen in Figure S5e−h. The 20 min MPPT condition used in this work is summarized in Table 2. In contrast, though the 5% excess FACl 1, 5, 10, and 20 min PSCs show low initial PCE, during the 20 min MPPT their PCEs keep increasing and eventually stabilize at a higher PCE. The PCE increase of 5% excess FACl 1 and 5 min are caused by both increase in V_{mpp} and current density at maximum power point (J_{mpp}) (Figure S5a,b), whereas the PCE increase of 5% excess FACl 10 and 20 min is due to J_{mpp} increase (Figure S5c,d). For instance, the 3.17% excess $PbCl_2$ 10 min PSC shows a high initial PCE of 18.6%. After 20 min MPPT, its PCE drops to 17.4%. Its J_{mpp} remains unchanged whereas V_{mpp} decreases from 0.88 to 0.83 V (Figure S5h). The PCE of 5% excess FACl 30 min PSC is initially 18.5% and it drops to 17.9% at the end of MPPT. Its J_{mpp} shows little change whereas

V_{mpp} decreases from 0.88 to 0.83 V (Figure S5e). On the contrary, the 5% excess FACl 20 min PSC shows a lower initial PCE of 17.2%. Its PCE keeps increasing to 19% in the first 10 min MPPT and then stabilizes at 19% till the end. Its V_{mpp} shows little change whereas J_{mpp} increased from 19.1 to 21.5 mA/cm^2 (Figure S5d). The calculated average PCE of 3.17% excess $PbCl_2$ 10 min, 5% excess FACl 30 min, and 5% excess FACl 20 min PSCs during the 20 min MPPT is 18.0%, 18.0%, and 18.7%, respectively. Thus, despite the lower initial PCE from the 5% excess FACl 20 min PSC, it generates more energy in 20 min than the other two PSCs. To demonstrate that the observed trend is reproducible, MPPT results of multiple 5% excess FACl 1−40 min PSCs are shown in Figure S6.

It appears that the perovskite films with Pb-rich surfaces result in declining PCE during MPPT, whereas the films with less Pb-rich surfaces lead to more stable PSCs during MPPT. To verify this discovery in longer term solar cell operation and under harsher conditions, we tracked the MPP of PSCs under 1 sun illumination from a metal halide lamp with strong UV content for 40 h. The long-term MPPT condition used in this work is summarized in Table 2. During this tracking, the cell temperatures reached 60 °C. As can be seen from Figure 4d, the stoichiometric 10 min and 3.17% excess $PbCl_2$ 10 min PSCs maintain less than 78% initial PCE. In contrast, the 5% excess FACl 10 and 20 min PSCs are much more stable, maintaining more than 91% initial PCE at the end of 40 h MPPT.

To further prove the above link between perovskite surface stoichiometry and the solar cell operational stability, we performed controlled experiments by changing the annealing temperature, the annealing time, AX species, and AX amount, then tracking their PCE during MPPT. First, we kept the FACl 5% excess and annealed it at 150 °C instead of 130 °C for 10 min to accelerate the FACl evaporation during annealing. This way, the surface of 5% excess FACl 150 °C 10 min perovskite
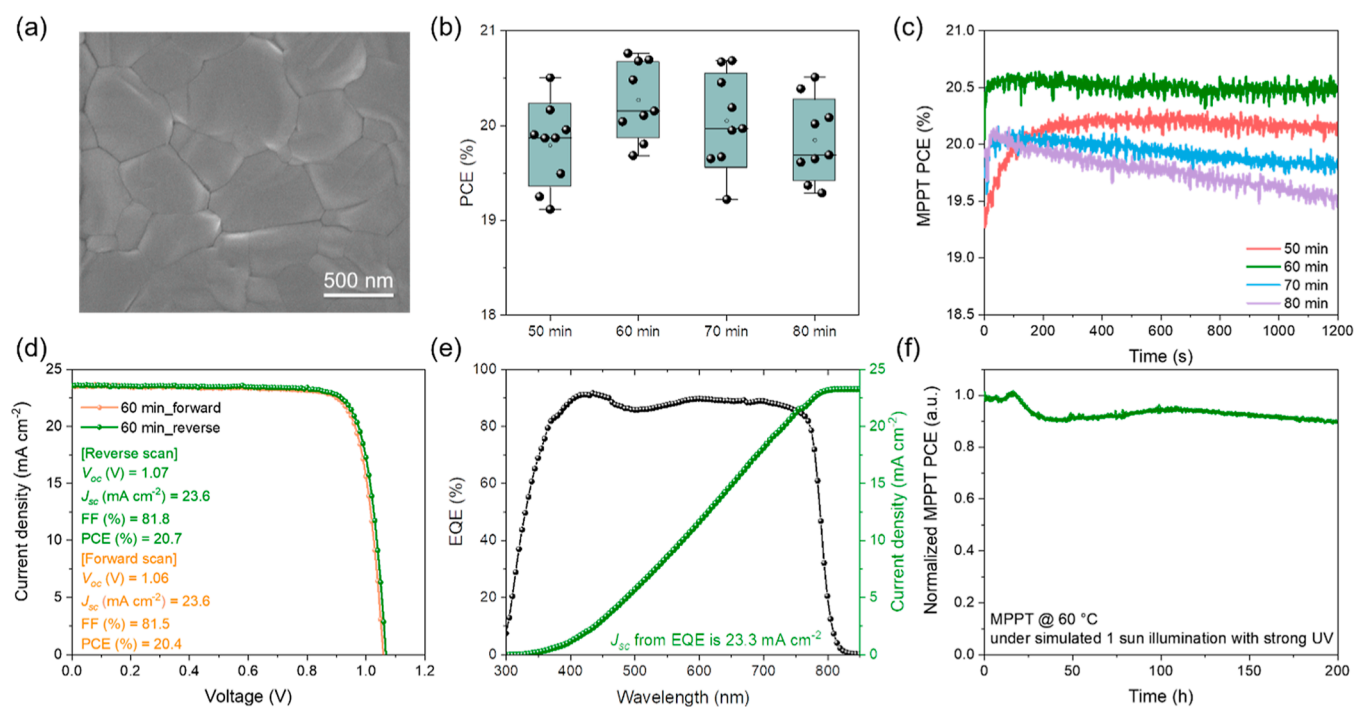
Figure 7. High-efficiency PSCs with 30% MACl additive. (a) Top-view SEM image of the perovskite film. The perovskite film was annealed at 110 °C for 60 min. (b) PCE distribution diagram of the corresponding gas quenched PSCs with different perovskite annealing time, including 50, 60, 70, and 80 min. (c) 20 min MPPT measurements of the corresponding PSCs. (d) $J-V$ curves of the champion device under reverse and forward scans. The inset shows the corresponding PV parameters. (e) EQE and integrated J_{sc} spectra of the champion device. (f) Operational stability test of the PSC based on the optimal condition. The test is carried out under simulated 1 sun illumination from a metal halide lamp with strong UV content. The cell temperature reaches 60 °C.

film will be more Pb-rich than the 5% excess FACl 130 °C 10 min film. As a result, the 150 °C 10 min film indeed shows declining PCE as indicated by the purple curve in Figure 6a. Then, we drastically increased the amount of FACl excess from 5 to 30% so that even at the end of a long-time annealing the FACl is not able to fully escape the films, potentially creating AX-rich perovskite films. Indeed, after annealing at 130 °C for 80 min, the PSC with this perovskite shows increasing PCE during MPPT as indicated by the blue curve in Figure 6a.

To follow up, we then replaced FACl additive with a less volatile FAI additive. As also shown in Figure 6a, with a limited amount of 1.5% excess FAI, the device behaves like the denoted stoichiometric device, for which the PCE degrades under MPPT tracking. Nevertheless, with the amount of excess FAI increasing to 2.5% and 5%, the device starts to show the opposite trend under MPPT tracking, that is, PCE first significantly increases and then stabilizes with tracking time. Interestingly, due to the much less volatile nature of FAI than FACl, the annealing time plays a marginal role in the case of FAI additive. In Figure S7, nearly identical initial PCEs and MPPT tracking behavior have been observed for the PSCs made with 5% excess FAI but annealed at 130 °C for 20, 40, and 60 min, respectively. Their PCEs all increase in the same fashion from below 2% to above 10% at the end of 20 min MPPT. The above controlled experiments clearly prove that despite low initial PCE, the AX-rich devices are more stable under MPPT.

Finally, we designed another experiment where the 5% excess FACl perovskite film was first annealed at 130 °C for 60 min to realize a Pb-rich surface. After this, we applied surface treatment on such films by spin-coating FAI solutions with different concentrations. Figure 6b shows that the 5% excess

FACl 130 °C 60 min PSC presents a typical declining MPPT PCE. However, as the FAI solution concentration of the surface treatment increases, the perovskite film turns from Pb-rich to less Pb-rich and eventually to AX-rich.[24] Correspondingly, Figure 6b shows that the device turns from having a declining MPPT PCE (pristine) to a more stable MPPT PCE (0.5 mg/mL) and then an increasing MPPT PCE (1.0 mg/mL).

To conclude, with the experimental results presented in this section, we can find a clear link between the perovskite film stoichiometry and the solar cell operational stability. Perovskites with Pb-rich surfaces result in high initial PCE but declining PCE during MPPT, whereas AX-rich perovskites lead to low initial PCE but increasing MPPT. Therefore, to be able to deliver both high initial PCE and stable MPPT PCE, a careful screening of annealing conditions including temperature and duration is needed when the volatile additive is present in the perovskite solution.

2.3. Verifying the Generality Using PSCs with MACl Additive. MACl is another commonly used additive for high-efficiency PSCs.[15−19] In order to verify the generality of the above-observed link between stoichiometry and device performance, we have done another case study, where 30 mol % MACl is used as the volatile AX additive in the perovskite precursor solution. The obtained perovskite precursor films were annealed at 110 °C for 50, 60, 70, and 80 min, respectively. Figure 7a shows the top-view SEM image of the perovskite with MACl additive that was annealed for 60 min. Compared to the one with FACl additive, much larger grain size is realized with MACl additive, which could be attributed to higher amount of chlorine used.[17] The device performance of the gas quenched inverted p−i−n PSCs was

evaluated with a configuration of ITO/PTAA/perovskite/LiF/C_{60}/BCP/Cu. The PCE distribution diagram is shown in Figure 7b and the other parameters are shown in Figure S8. Interestingly, the average PCEs of the devices do not vary significantly with perovskite annealing time, though the devices prepared with films annealed for 60 min show a slightly higher average PCE. However, as displayed in Figure 7c, we can find the same link between the annealing time and MPPT behavior as what is shown in the case of perovskite films fabricated with FACl additive. When the perovskite film is annealed for a relatively short time, that is 50 min, the corresponding device's MPPT PCE takes about 5 min to increase from the initial 19.3% to a stabilized 20.1%. When an optimal annealing time is applied, that is 60 min, we can obtain the highest and the most stable MPPT PCE of 20.5% during the 20 min tracking time. Once the perovskite film is over annealed, that is, in the case of 70 and 80 min, the MPPT PCE keeps decreasing during the measurement. In particular, the longer the annealing time is, the more remarkable decrease in MPPT PCE is observed. Similar to the case of FACl, a prolonged annealing time will result in perovskite films with Pb-rich surfaces because MACl is even more volatile. As discussed above, it is important to carefully control the annealing temperature and duration to achieve high and stable MPPT PCEs. By annealing the precursor films with MACl additive at 110 °C for 60 min, we can achieve the best device performance with negligible hysteresis (Figure 7d) and high EQE that leads to an integrated J_{sc} of 23.3 mA cm^{-2} (Figure 7e). More importantly, the device can maintain approximately 90% of the initial performance after 200 h MPPT at 60 °C under 1 sun illumination from a metal halide lamp with strong UV content.

3. CONCLUSIONS

To conclude, our work reveals the stoichiometry of perovskite films that contain volatile AX additives that can be readily controlled by changing their thermal annealing temperature and time. We then unraveled how such volatile additives can influence the perovskite film stoichiometry and how this correlates to the device performance and operational stability. It is discovered that the over annealed perovskite films become Pb-rich at the surface, leading to PSCs with high initial PCE but poor stability under MPPT condition. On the contrary, the under annealed films lead to PSCs with low initial PCEs, but the PCEs increase during MPPT. We verified the generality of this by studying perovskite precursors using either FACl or MACl as an additive, showing it is important to control the annealing conditions to simultaneously achieve high efficiency and operational stability. With optimally annealed perovskite films, we demonstrated efficient and stable p−i−n PSCs that show the best PCE of 20.7% and remain 90% of the initial performance after a 200 h MPPT at 60 °C under 1 sun illumination with high UV content. Therefore, this work provides a new guideline for the fabrication of high-efficiency and operationally stable PSCs.

4. EXPERIMENTAL SECTION

4.1. Materials and Fabrication Details. *4.1.1. Materials.* The materials used in this work and the companies that supplied them are listed in Table 1.

4.1.2. Solution Preparation. 4.1.2.1. PTAA Solution. Dissolve 2 mg of PTAA in 1 mL of anhydrous toluene.

4.1.2.2. $Cs_{0.1}FA_{0.9}PbI_{2.865}Br_{0.135}$ Precursor Solution. Dissolve 1.2450 mmol PbI$_2$, 0.1245 mmol CsI, 0.9524 mmol FAI, and 0.1681 mmol

FABr in 1 mL of mixed solvents composed of 0.9 mL of DMF and 0.1 mL of NMP. Stir the solution at room temperature until all powder dissolves.

4.1.2.3. $Cs_{0.1}FA_{0.9}PbI_{2.865}Br_{0.135}$ + 3.17% PbCl$_2$ Precursor Solution. Add 0.0395 mmol PbCl$_2$ in a solution as described in section 4.1.2.2.

4.1.2.4. $Cs_{0.1}FA_{0.9}PbI_{2.865}Br_{0.135}$ + 5% FACl Precursor Solution. Dissolve 1.2139 mmol PbI$_2$, 0.0311 mmol PbCl$_2$, 0.1245 mmol CsI, 1.0147 mmol FAI, and 0.1681 mmol FABr in 1 mL of mixed solvents composed of 0.9 mL of DMF and 0.1 mL of NMP. Stir the solution at room temperature until all powder dissolves.

4.1.2.5. $Cs_{0.1}FA_{0.9}PbI_{2.865}Br_{0.135}$ + 30% MACl Precursor Solution. Dissolve 0.07424 mmol PbBr$_2$, 1.02575 mmol PbI$_2$, 0.99 mmol FAI. 0.11 mmol CsI and 0.33 mmol MACl in 1 mL mixed solvents composed of 0.9 mL DMF and 0.1 mL NMP. Stir the solution at room temperature until all powder dissolves.

4.1.3. Device Fabrication. The ITO-coated glass substrates were subsequently cleaned for 5 min in an ultrasonic bath of detergent, deionized water, acetone, and isopropanol. Afterward, they were transferred to a nitrogen-filled glovebox for material depositions. 100 μL of PTAA solution was dynamically spin-coated on the substrate at 5500 rpm for 35 s, after which the PTAA layer was annealed at 100 °C for 10 min. After cooling down the sample, 100 μL of perovskite precursor solution was dynamically spin-coated on PTAA by a continuous two-step program, first 2000 rpm for 10 s and then 5000 rpm for 45 s. During this coating process, the perovskite film was quenched with nitrogen for 30 s, starting at 40 s prior to the end of the program. Then, the perovskite films were annealed at the corresponding temperatures and durations mentioned in the article. After the samples cooled to room temperature, the samples made from stoichiometric, excess FACl, and excess PbCl$_2$ perovskite solutions were transferred into a high-vacuum chamber (base pressure ~ 10^{-7} Torr) to deposit 40 nm C$_{60}$ (0.5 Å/s) and 5 nm BCP (0.5 Å/s) by thermal evaporation. For the samples made from excess MACl perovskite solutions, 0.8 nm LiF (0.1 Å/s) was evaporated prior to 20 nm C$_{60}$ (0.5 Å/s) and 5 nm BCP (0.5 Å/s). Afterward, a 100 nm thick copper (Cu) layer was thermally evaporated at the rate of 2 Å/s. The active cell area of 0.13 cm^2 is defined by a metal mask. For the excess MACl solar cells, 120 nm of MgF$_2$ was evaporated at the rate of 2 Å/s on the glass side.

4.2. Characterizations and Analysis. *4.2.1. Current−Voltage Measurement.* IV measurements were performed in a nitrogen-filled glovebox using a Keithley 2602A source-measure unit and an Abet solar simulator with simulated 100 mW/cm^2 AM1.5G illumination from a 450 W xenon lamp (Abet Sun 3000). A fan was implemented to keep the PSC temperature at 30 °C. The illumination intensity was calibrated with a Fraunhofer ISE's WPVS reference solar cell (Type: RS-ID-4). The solar cells were measured between −0.2 and 1.2 V with a voltage step of 0.01 V and a delay time of either 0.01 or 0.1 s.

4.2.3. Maximum Power Point Tracking. The 20 min MPPT was conducted in the Abet solar simulator mentioned above. We followed the "Tracking algorithm" from our previous work by Rakocevic et al.[36]

The long-term MPPT was conducted in a N$_2$-filled glovebox under 1 sun illumination from a metal halide lamp with AM1.5G spectrum (containing stronger UV light compared to a xenon lamp). Due to the heating, the samples reach temperatures of 60 °C. The samples were tracked by a maximum power point tracker with a perturb and observe algorithm that adjusted the maximum power voltage every 60 s.

The MPPT conditions are summarized in the following table according to the suggestion from Khenkin et al.[37]

4.2.4. Scanning Electron Microscopy. The SEM images are acquired with a Zeiss Gemini 450 field emission scanning electron microscope. The article contains images from the in-chamber secondary electron detector and the in-lens detector.

4.2.5. X-Ray Diffraction. The XRD study is performed with a Bruker D8 goniometer equipped with a Göble mirror and a 1D LYNXEYE detector using Cu Kα radiation.

Lattice constants of the perovskite films shown in Figure 3a are average of lattice constants calculated based on peaks (001), (002), and (012) using formula

$$d_{hkl} = \lambda/2 \sin \theta \tag{1}$$

$$1/d_{hkl} = h^2 + k^2 + l^2/a^2 \tag{2}$$

where h, k, and l are miller indices, λ is the wavelength of X-ray and in this case is 1.54184 Å from Cu Kα radiation, a is the lattice constant, and θ is the angle between the incident beam and the normal of the entrance surface.

4.2.6. X-Ray Photoelectron Spectroscopy. The measurements were carried out in the angle-integrated mode using a QUANTES instrument from Physical Electronics. The measurements were performed using a monochromatized photon beam of 1486.6 eV. A 100 microns spot was used. Charge neutralization was used during this experiment.

Sensitivity factors specific for each instrument were used to convert peak areas to atomic concentrations. As a result of this, it is possible that the concentrations deviate from reality in the absolute sense (generally not more than 20% relative). When atomic concentrations of XPS results are compared with each other, however, the results are more accurate. All data presented are for the 45° exit angle.

4.2.7. Photoluminescence. The steady-state PL measurements were performed on PicoQuant FluoTime 300 under ambient conditions.

4.2.8. Calculation of Average PCE Based on MPPT Data. In Section 2.2, the average PCEs of 3.17% excess PbCl$_2$ 10 min, 5% excess FACl 30 min, and 5% excess FACl 20 min PSCs during the 20 min MPPT are calculated. The average PCEs are calculated using the following equation, where t is the time in the unit of seconds

$$\text{average PCE} = \int_{0}^{1200} \text{PCE}(t)\mathrm{d}t/1200 \tag{3}$$

■ ASSOCIATED CONTENT

Ⓢ Supporting Information

The Supporting Information is available free of charge at https://pubs.acs.org/doi/10.1021/acsami.2c05241.

Additional experimental details including SEM, PL, JV, and MPPT results (PDF)

■ AUTHOR INFORMATION

Corresponding Authors

Weiming Qiu − *imec, Leuven 3001, Belgium;*
Email: Weiming.Qiu@imec.be

Yinghuan Kuang − *Thin Film PV Technology—Partner in Solliance, Imec, Genk 3600, Belgium; EnergyVille, Genk 3600, Belgium; Hasselt University, Hasselt 3500, Belgium;*
Email: Yinghuan.Kuang@imec.be

Jef Poortmans − *Department of Electrical Engineering (ESAT), Katholieke Universiteit Leuven, 3001 Leuven, Belgium; Thin Film PV Technology—Partner in Solliance, Imec, Genk 3600, Belgium; EnergyVille, Genk 3600, Belgium; Hasselt University, Hasselt 3500, Belgium;*
Email: Jef.Poortmans@imec.be

Authors

Wenya Song − *Department of Electrical Engineering (ESAT), Katholieke Universiteit Leuven, 3001 Leuven, Belgium; Thin Film PV Technology—Partner in Solliance, Imec, Genk 3600, Belgium; EnergyVille, Genk 3600, Belgium; Hasselt University, Hasselt 3500, Belgium;* orcid.org/0000-0003-1988-9324

Xin Zhang − *Department of Electrical Engineering (ESAT), Katholieke Universiteit Leuven, 3001 Leuven, Belgium; Thin Film PV Technology—Partner in Solliance, Imec, Genk 3600, Belgium; EnergyVille, Genk 3600, Belgium; Hasselt University, Hasselt 3500, Belgium; Center for Micro Nano Systems, School of Information Science and Technology (SIST), Fudan University, Shanghai 200433, P. R. China; Academy for Engineering & Technology (FAET), Fudan University, 200433 Shanghai, P. R. China;* orcid.org/0000-0002-2228-3633

Stijn Lammar − *Department of Electrical Engineering (ESAT), Katholieke Universiteit Leuven, 3001 Leuven, Belgium; Thin Film PV Technology—Partner in Solliance, Imec, Genk 3600, Belgium; EnergyVille, Genk 3600, Belgium; Hasselt University, Hasselt 3500, Belgium*

Bart Ruttens − *Hasselt University, Hasselt 3500, Belgium*

Jan D'Haen − *Hasselt University, Hasselt 3500, Belgium*

Inge Vaesen − *imec, Leuven 3001, Belgium*

Thierry Conard − *imec, Leuven 3001, Belgium*

Yaser Abdulraheem − *Department of Electrical Engineering, Kuwait University, Safat 13060, Kuwait*

Tom Aernouts − *Thin Film PV Technology—Partner in Solliance, Imec, Genk 3600, Belgium; EnergyVille, Genk 3600, Belgium; Hasselt University, Hasselt 3500, Belgium*

Yiqiang Zhan − *Center for Micro Nano Systems, School of Information Science and Technology (SIST), Fudan University, Shanghai 200433, P. R. China; Academy for Engineering & Technology (FAET), Fudan University, 200433 Shanghai, P. R. China;* orcid.org/0000-0001-8391-2555

Complete contact information is available at:
https://pubs.acs.org/10.1021/acsami.2c05241

Author Contributions

○W.S., X.Z., and S.L. contributed equally to this work.

Notes

The authors declare no competing financial interest.

■ ACKNOWLEDGMENTS

■ REFERENCES

(1) Best Research-Cell Efficiencies NREL. https://www.nrel.gov/pv/assets/pdfs/best-research-cell-efficiencies-rev220126b.pdf , accessed June 9th, 2022.

(2) Jeong, J.; Kim, M.; Seo, J.; Lu, H.; Ahlawat, P.; Mishra, A.; Yang, Y.; Hope, M. A.; Eickemeyer, F. T.; Kim, M.; Yoon, Y. J.; Choi, I. W.; Darwich, B. P.; Choi, S. J.; Jo, Y.; Lee, J. H.; Walker, B.; Zakeeruddin, S. M.; Emsley, L.; Rothlisberger, U.; Hagfeldt, A.; Kim, D. S.; Grätzel, M.; Kim, J. Y. Pseudo-Halide Anion Engineering for α-FAPbI$_3$ Perovskite Solar Cells. *Nature* **2021**, *592*, 381−385.

(3) Min, H.; Lee, D. Y.; Kim, J.; Kim, G.; Lee, K. S.; Kim, J.; Paik, M. J.; Kim, Y. K.; Kim, K. S.; Kim, M. G.; Shin, T. J.; Il Seok, S. Perovskite Solar Cells with Atomically Coherent Interlayers on SnO$_2$ Electrodes. *Nature* **2021**, *598*, 444−450.

(4) Yoo, J. J.; Seo, G.; Chua, M. R.; Park, T. G.; Lu, Y.; Rotermund, F.; Kim, Y.-K.; Moon, C. S.; Jeon, N. J.; Correa-Baena, J.-P.; Bulović, V.; Shin, S. S.; Bawendi, M. G.; Seo, J. Efficient Perovskite Solar Cells via Improved Carrier Management. *Nature* **2021**, *590*, 587−593.

(5) Li, N.; Niu, X.; Li, L.; Wang, H.; Huang, Z.; Zhang, Y.; Chen, Y.; Zhang, X.; Zhu, C.; Zai, H.; Bai, Y.; Ma, S.; Liu, H.; Liu, X.; Guo, Z.; Liu, G.; Fan, R.; Chen, H.; Wang, J.; Lun, Y.; Wang, X.; Hong, J.; Xie, H.; Jakob, D. S.; Xu, X. G.; Chen, Q.; Zhou, H. Liquid Medium Annealing for Fabricating Durable Perovskite Solar Cells with Improved Reproducibility. *Science* **2021**, *373*, 561−567.

(6) Deng, Y.; Xu, S.; Chen, S.; Xiao, X.; Zhao, J.; Huang, J. Defect Compensation in Formamidinium−Caesium Perovskites for Highly Efficient Solar Mini-Modules with Improved Photostability. *Nat. Energy* **2021**, *6*, 633−641.

(7) Li, N.; Tao, S.; Chen, Y.; Niu, X.; Onwudinanti, C. K.; Hu, C.; Qiu, Z.; Xu, Z.; Zheng, G.; Wang, L.; Zhang, Y.; Li, L.; Liu, H.; Lun, Y.; Hong, J.; Wang, X.; Liu, Y.; Xie, H.; Gao, Y.; Bai, Y.; Yang, S.; Brocks, G.; Chen, Q.; Zhou, H. Cation and Anion Immobilization through Chemical Bonding Enhancement with Fluorides for Stable Halide Perovskite Solar Cells. *Nat. Energy* **2019**, *4*, 408−415.

(8) Wang, L.; Zhou, H.; Hu, J.; Huang, B.; Sun, M.; Dong, B.; Zheng, G.; Huang, Y.; Chen, Y.; Li, L.; Xu, Z.; Li, N.; Liu, Z.; Chen, Q.; Sun, L.-D.; Yan, C.-H. A Eu^{3+}-Eu^{2+} Ion Redox Shuttle Imparts Operational Durability to Pb-I Perovskite Solar Cells. *Science* **2019**, *363*, 265−270.

(9) Fassl, P.; Lami, V.; Bausch, A.; Wang, Z.; Klug, M. T.; Snaith, H. J.; Vaynzof, Y. Fractional Deviations in Precursor Stoichiometry Dictate the Properties, Performance and Stability of Perovskite Photovoltaic Devices. *Energy Environ. Sci.* **2018**, *11*, 3380−3391.

(10) Juarez-Perez, E. J.; Hawash, Z.; Raga, S. R.; Ono, L. K.; Qi, Y. Thermal Degradation of $CH_3NH_3PbI_3$ Perovskite into NH_3 and CH_3I Gases Observed by Coupled Thermogravimetry-Mass Spectrometry Analysis. *Energy Environ. Sci.* **2016**, *9*, 3406−3410.

(11) Juarez-Perez, E. J.; Ono, L. K.; Maeda, M.; Jiang, Y.; Hawash, Z.; Qi, Y. Photodecomposition and Thermal Decomposition in Methylammonium Halide Lead Perovskites and Inferred Design Principles to Increase Photovoltaic Device Stability. *J. Mater. Chem. A* **2018**, *6*, 9604−9612.

(12) Tavakoli, M. M.; Yadav, P.; Prochowicz, D.; Sponseller, M.; Osherov, A.; Bulović, V.; Kong, J. Controllable Perovskite Crystallization via Antisolvent Technique Using Chloride Additives for Highly Efficient Planar Perovskite Solar Cells. *Adv. Energy Mater.* **2019**, *9*, 1803587.

(13) Dagar, J.; Fenske, M.; Al-Ashouri, A.; Schultz, C.; Li, B.; Köbler, H.; Munir, R.; Parmasivam, G.; Li, J.; Levine, I.; Merdasa, A.; Kegelmann, L.; Näsström, H.; Marquez, J. A.; Unold, T.; Többens, D. M.; Schlatmann, R.; Stegemann, B.; Abate, A.; Albrecht, S.; Unger, E. Compositional and Interfacial Engineering Yield High-Performance and Stable p-i-n Perovskite Solar Cells and Mini-Modules. *ACS Appl. Mater. Interfaces* **2021**, *13*, 13022−13033.

(14) Prochowicz, D.; Runjhun, R.; Tavakoli, M. M.; Yadav, P.; Saski, M.; Alanazi, A. Q.; Kubicki, D. J.; Kaszkur, Z.; Zakeeruddin, S. M.; Lewiński, J.; Grätzel, M. Engineering of Perovskite Materials Based on Formamidinium and Cesium Hybridization for High-Efficiency Solar Cells. *Chem. Mater.* **2019**, *31*, 1620−1627.

(15) Kim, M.; Kim, G.-H.; Lee, T. K.; Choi, I. W.; Choi, H. W.; Jo, Y.; Yoon, Y. J.; Kim, J. W.; Lee, J.; Huh, D.; Lee, H.; Kwak, S. K.; Kim, J. Y.; Kim, D. S. Methylammonium Chloride Induces Intermediate Phase Stabilization for Efficient Perovskite Solar Cells. *Joule* **2019**, *3*, 2179−2192.

(16) Mateen, M.; Arain, Z.; Yang, Y.; Liu, X.; Ma, S.; Liu, C.; Ding, Y.; Ding, X.; Cai, M.; Dai, S. MACl-Induced Intermediate Engineering for High-Performance Mixed-Cation Perovskite Solar Cells. *ACS Appl. Mater. Interfaces* **2020**, *12*, 10535−10543.

(17) Odysseas Kosmatos, K.; Theofylaktos, L.; Giannakaki, E.; Deligiannis, D.; Konstantakou, M.; Stergiopoulos, T. Methylammonium Chloride: A Key Additive for Highly Efficient, Stable, and Up-Scalable Perovskite Solar Cells. *Energy Environ. Mater.* **2019**, *2*, 79−92.

(18) Gutierrez-Partida, E.; Hempel, H.; Caicedo-Dávila, S.; Raoufi, M.; Peña-Camargo, F.; Grischek, M.; Gunder, R.; Diekmann, J.; Caprioglio, P.; Brinkmann, K. O.; Köbler, H.; Albrecht, S.; Riedl, T.; Abate, A.; Abou-Ras, D.; Unold, T.; Neher, D.; Stolterfoht, M. Large-Grain Double Cation Perovskites with 18 μs Lifetime and High Luminescence Yield for Efficient Inverted Perovskite Solar Cells. *ACS Energy Lett.* **2021**, *6*, 1045−1054.

(19) Xiong, Z.; Lan, L.; Wang, Y.; Lu, C.; Qin, S.; Chen, S.; Zhou, L.; Zhu, C.; Li, S.; Meng, L.; Sun, K.; Li, Y. Multifunctional Polymer Framework Modified SnO2 Enabling a Photostable α-FAPbI3 Perovskite Solar Cell with Efficiency Exceeding 23%. *ACS Energy Lett.* **2021**, *6*, 3824−3830.

(20) Tan, W. L.; Choo, Y. Y.; Huang, W.; Jiao, X.; Lu, J.; Cheng, Y.-B.; McNeill, C. R. Oriented Attachment as the Mechanism for Microstructure Evolution in Chloride-Derived Hybrid Perovskite Thin Films. *ACS Appl. Mater. Interfaces* **2019**, *11*, 39930−39939.

(21) Roose, B.; Dey, K.; Chiang, Y.-H.; Friend, R. H.; Stranks, S. D. Critical Assessment of the Use of Excess Lead Iodide in Lead Halide Perovskite Solar Cells. *J. Phys. Chem. Lett.* **2020**, *11*, 6505−6512.

(22) Kuang, Y.; Zardetto, V.; Van Gils, R.; Karwal, S.; Koushik, D.; Verheijen, M. A.; Black, L. E.; Weijtens, C.; Veenstra, S.; Andriessen, R.; Kessels, W. M. M.; Creatore, M. Low-Temperature Plasma-Assisted Atomic-Layer-Deposited SnO$_2$ as an Electron Transport Layer in Planar Perovskite Solar Cells. *ACS Appl. Mater. Interfaces* **2018**, *10*, 30367−30378.

(23) Wang, H.; Wang, Z.; Yang, Z.; Xu, Y.; Ding, Y.; Tan, L.; Yi, C.; Zhang, Z.; Meng, K.; Chen, G.; Zhao, Y.; Luo, Y.; Zhang, X.; Hagfeldt, A.; Luo, J. Ligand-Modulated Excess PbI$_2$ Nanosheets for Highly Efficient and Stable Perovskite Solar Cells. *Adv. Mater.* **2020**, *32*, 2000865.

(24) Hu, Z.; An, Q.; Xiang, H.; Aigouy, L.; Sun, B.; Vaynzof, Y.; Chen, Z. Enhancing the Efficiency and Stability of Triple-Cation Perovskite Solar Cells by Eliminating Excess PbI$_2$ from the Perovskite/Hole Transport Layer Interface. *ACS Appl. Mater. Interfaces* **2020**, *12*, 54824−54832.

(25) Xie, L.-Q.; Chen, L.; Nan, Z.-A.; Lin, H.-X.; Wang, T.; Zhan, D.-P.; Yan, J.-W.; Mao, B.-W.; Tian, Z.-Q. Understanding the Cubic Phase Stabilization and Crystallization Kinetics in Mixed Cations and Halides Perovskite Single Crystals. *J. Am. Chem. Soc.* **2017**, *139*, 3320−3323.

(26) Sun, Y.; Peng, J.; Chen, Y.; Yao, Y.; Liang, Z. Triple-Cation Mixed-Halide Perovskites: Towards Efficient, Annealing-Free and Air-Stable Solar Cells Enabled by Pb(SCN)$_2$ Additive. *Sci. Rep.* **2017**, *7*, 46193.

(27) Chen, S.; Pan, L.; Ye, T.; Lei, N.; Yang, Y.; Wang, X. The Lattice Reconstruction of Cs-Introduced FAPbI$_{1.80}$Br$_{1.20}$ Enables Improved Stability for Perovskite Solar Cells. *RSC Adv.* **2021**, *11*, 3997−4005.

(28) Zhou, N.; Shen, Y.; Zhang, Y.; Xu, Z.; Zheng, G.; Li, L.; Chen, Q.; Zhou, H. CsI Pre-Intercalation in the Inorganic Framework for Efficient and Stable FA$_{1−x}$Cs$_x$PbI$_3$(Cl) Perovskite Solar Cells. *Small* **2017**, *13*, 1700484.

(29) Belarbi, E.; Vallés-Pelarda, M.; Clasen Hames, B.; Sanchez, R. S.; Barea, E. M.; Maghraoui-Meherzi, H.; Mora-Seró, I. Transformation of PbI$_2$, PbBr$_2$ and PbCl$_2$ Salts into MAPbBr$_3$ Perovskite by Halide Exchange as an Effective Method for Recombination Reduction. *Phys. Chem. Chem. Phys.* **2017**, *19*, 10913−10921.

(30) Condeles, J. F.; Lofrano, R.; Rosolen, J. M.; Mulato, M. Stoichiometry, Surface and Structural Characterization of Lead Iodide Thin Films. *Braz. J. Phys.* **2006**, *36*, 320−323.

(31) Condeles, J. F.; Ando, R. A.; Mulato, M. Optical and Structural Properties of PbI$_2$ Thin Films. *J. Mater. Sci.* **2008**, *43*, 525−529.

(32) *NIST X-Ray Photoelectron Database*; version 4.1, National Institute of Standards and Technology: Gaithersburg, 2012 https://srdata.nist.gov/xps/faq.aspx (accessed 2021 11 22).

(33) McGettrick, J. D.; Hooper, K.; Pockett, A.; Baker, J.; Troughton, J.; Carnie, M.; Watson, T. Sources of Pb(0) Artefacts during XPS Analysis of Lead Halide Perovskites. *Mater. Lett.* **2019**, *251*, 98−101.

(34) Plekhanov, V. G. Lead Halides: Electronic Properties and Applications. *Prog. Mater. Sci.* **2004**, *49*, 787−886.

(35) Yuan, Y.; Xu, R.; Xu, H.-T.; Hong, F.; Xu, F.; Wang, L.-J. Nature of the Band Gap of Halide Perovskites ABX$_3$ (A = CH_3NH_3,

Cs; B = Sn, Pb; X = Cl, Br, I): First-Principles Calculations. *Chin. Phys. B* **2015**, *24*, 116302.

(36) Rakocevic, L.; Ernst, F.; Yimga, N. T.; Vashishtha, S.; Aernouts, T.; Heumueller, T.; Brabec, C. J.; Gehlhaar, R.; Poortmans, J. Reliable Performance Comparison of Perovskite Solar Cells Using Optimized Maximum Power Point Tracking. *Sol. RRL* **2019**, *3*, 1800287.

(37) Khenkin, M. V.; Katz, E. A.; Abate, A.; Bardizza, G.; Berry, J. J.; Brabec, C.; Brunetti, F.; Bulović, V.; Burlingame, Q.; Di Carlo, A.; Cheacharoen, R.; Cheng, Y.-B.; Colsmann, A.; Cros, S.; Domanski, K.; Dusza, M.; Fell, C. J.; Forrest, S. R.; Galagan, Y.; Di Girolamo, D.; Grätzel, M.; Hagfeldt, A.; von Hauff, E.; Hoppe, H.; Kettle, J.; Köbler, H.; Leite, M. S.; Liu, S.; Loo, Y.-L.; Luther, J. M.; Ma, C.-Q.; Madsen, M.; Manceau, M.; Matheron, M.; McGehee, M.; Meitzner, R.; Nazeeruddin, M. K.; Nogueira, A. F.; Odabaşı, Ç.; Osherov, A.; Park, N.-G.; Reese, M. O.; De Rossi, F.; Saliba, M.; Schubert, U. S.; Snaith, H. J.; Stranks, S. D.; Tress, W.; Troshin, P. A.; Turkovic, V.; Veenstra, S.; Visoly-Fisher, I.; Walsh, A.; Watson, T.; Xie, H.; Yıldırım, R.; Zakeeruddin, S. M.; Zhu, K.; Lira-Cantu, M. Consensus Statement for Stability Assessment and Reporting for Perovskite Photovoltaics Based on ISOS Procedures. *Nat. Energy* **2020**, *5*, 35−49.